Atmospheric Pressure Coated-Wall Flow-Tube Study of Acetone Adsorption on Ice

Thorsten Bartels-Rausch,*,† Thomas Huthwelker, Heinz W. Gäggeler,‡ and Markus Ammann*

Paul Scherrer Institute, 5232 Villigen PSI, Switzerland

Received: October 21, 2004; In Final Form: February 9, 2005

An atmospheric pressure variant of the coated-wall flow-tube technique in combination with a Monte Carlo simulation is presented. In a performance test of simple first-order wall loss, the Monte Carlo simulation, which uses a simplified model of transport in laminar flow, reproduced results of an analytical solution of the transport equations in a flow tube. This technique was then used to investigate the reversible adsorption of acetone on ice films between 203 and 223 K and a surface coverage of below 5% of a formal monolayer. Simulation of the experimental uptake traces allowed retrieving an adsorption enthalpy of -46 ± 3 kJ mol^{-1} for acetone on ice, which is in good agreement with other static and flow-tube methods. For the experimental conditions adopted here, the transport of acetone molecules along the ice film is governed by equilibrium thermodynamics. Therefore, the surface accommodation coefficient, S_0, and the preexponential factor, τ_0, for the activated desorption cannot be independently determined. These two main microphysical parameters describing partitioning can rather be estimated through their relation to the adsorption entropy. A first estimate for S_0 of acetone on ice in the range of 0.004−0.043 is given.

Introduction

There is strong evidence, both from field measurements[1] and laboratory experiments,[2] that ice and snow surfaces modify the atmospheric composition and consequently play a role in many atmospheric processes such as ozone depletion in the stratosphere,[3] ozone and hydroxide radical budget in the upper troposphere,[4] snowpack chemistry in the Arctic,[5,6] and associated processes such as halogen release associated with ozone and mercury depletion events.[7,8]

Acetone is of interest in atmospheric chemistry, because it is an important radical (HO_x) source in the upper troposphere[4] and a key player in the radical chemistry in the polar snowpack. Acetone is next to formaldehyde, an important intermediate in the atmospheric oxidation of organic compounds above snow, and both are important sources of HO_x, which largely determine the lifetime of trace gases in the near-surface polar air.[6] Its concentration, for which diurnal cycles have been observed in the near-surface polar air, is affected by local chemistry, the exchange of acetone with the snowpack, and also long-range transport processes.[9−12]

A major goal of laboratory research related to these issues is to quantify the various basic physiochemical parameters determining the uptake and reaction kinetics on ice surfaces. During the past 20 years or so, a number of methods have been developed for this purpose, such as the Knudsen cell,[13−15] molecular diffusion tube,[16] coated-wall flow tube,[17,18] and packed bed/chromatography-type experiments.[19−25] Due to the absence of collisions of molecules in the gas phase, the Knudsen cell allows a very accurate determination of the flux of molecules to a well-defined surface, especially for fast uptake kinetics. Many key experiments to elucidate processes on ice of stratospheric relevance have been performed in the Knudsen cell.[13] Yet, the significant vapor pressure of ice limits the use of Knudsen cells in this context to studies at temperatures below about 200 K. The molecular diffusion tube, in which the gas-phase molecules travel along a tube under molecular flow conditions, allows tracking the fate of the molecules after a large number of collisions. Consequently, slow uptake kinetics and surface residence times can be nicely addressed at pressures where the mean free path of the molecules in the gas phase is significantly larger than the tube dimensions. A higher vapor pressure of ice can be accommodated in the coated-wall flow-tube technique operating typically in the range of 1−50 Torr. The disadvantage of the higher pressure is the growing limitation of transport to the tube wall by gas-phase diffusion which limits kinetic investigations to slow uptake processes. Nevertheless, this technique has been successfully used for a number of reactive and nonreactive heterogeneous systems, including warmer ice under tropospheric conditions.[26−30] Also, the relative ease with which reasonably well-defined ice films may be introduced may be worthwhile being noted for this method. A variation is the chromatography-type flow tubes, in which ice is used in the form of a "packed bed" rather than a thin film, allowing the exposure of ice even in the form of natural snow samples[21,22,31] or proxies of snow at any temperature of interest. Retrieval of kinetic parameters is hampered by complex mixing/advection to the surface, and as in the flow tube, only slow processes with time scales much slower than the mixing time within the packing can be can be investigated kinetically. In both the coated-wall flow tube and the packed ice bed, equilibrium partitioning can be nicely measured, even in the presence of gas-phase diffusive limitations, simply by integration of the total loss to the solid phase. Slow processes, such as diffusion into the bulk, can be retrieved with experiments that run over long enough time scales.[32,33] For a review covering recent laboratory research on atmosphere−ice interactions and pointing out advantages and drawbacks of some of the above-mentioned methods, we refer to Abbatt.[34]

* Authors to whom correspondence should be addressed. E-mail: tbartels@chem.utoronto.ca; markus.ammann@psi.ch.

† Present address: Department of Chemistry, University of Toronto, 80 St. George Street, Toronto, ON M5S 3H6, Canada.

‡ Also at the University of Berne, 3008 Bern, Switzerland.

10.1021/jp045187l CCC: $30.25
Published on Web 04/30/2005

Here, we present a slightly different approach to investigate the nonreactive and nondiffusive partitioning of atmospheric trace gases between ice and air at low surface coverage, by using a coated-wall flow tube with its well-defined laminar flow profile to record frontal chromatograms at atmospheric pressure as typically used in chromatography-type flow tubes. In some aspects, this is a high-pressure extension of the molecular diffusion tube, where only straight trajectories between encounters with the wall occur. Since the 1970s, both methods (vacuum and high pressure) have also been used extensively in radiochemistry to describe separation of radioisotopes in gas chromatography.[35,36]

While the total uptake in a flow tube can be measured by integrating the breakthrough curve, the interpretation of the experimentally observed uptake kinetics requires some treatment of the gas-phase transport in the flow tube. The key problem, when evaluating experiments in a tubular flow reactor, is the correct coupling of the basic processes governing transport along the tube, i.e., adsorption to the surface, desorption from the surface, diffusion, and transport in the laminar flow. Several approaches, using different approximations, have been made to tackle this problem.[37−43] To model high uptake onto the tube surface, it was assumed that the gas-phase concentration at the tube walls vanishes.[37] The tube wall can also be described by the resistor boundary condition. Here, the flux to the tube wall is given by the difference of a desorbing and an adsorbing flux.[44,45] The third approach is to assume a first-order reaction at the tube wall but no desorbing flux back to the gas phase from the tube walls in various geometries.[41,42,46,47] Such solutions are often directed to specific geometries and boundary conditions and usually involve a series expansion or iterative procedures, such as the frequently used FORTRAN routine by Brown to treat first-order loss processes on walls.[42]

Using a statistical approach, Zvára[43] tackled this complex problem using a Monte Carlo model, which takes advantage of analytical solutions developed to describe the transport in a flow tube. We have extended this model to the question of atmospheric trace gas−ice interactions, including a parametrization of the adsorption and desorption processes appropriate in this context[48] and of diffusion and transport in laminar flow.[43] This is to our knowledge the first approach in which the diffusion in the gas phase of the experimental setup is explicitly treated. Recent approaches to simulate the transport of trace gases in coated-wall flow tubes[49] or Knudsen cells[50] have been developed for the molecular flow regime and consequently do not treat diffusion processes. Also, the theoretical framework presented here allows the assessment of necessary simulation parameters based on previous independent measurements. In previous works, these parameters have frequently been chosen arbitrarily.[49] While in principle the simulation problem posed here could also be solved by a numerical solution of the continuum problem, the Monte Carlo simulation is faster and, most importantly, much easier to handle, which makes the implementation of extensions for further processes in the condensed phase straightforward.

The acetone−ice interaction has been studied previously[29−31,51−53] due to its pronounced relevance in the atmosphere. The aim of this paper is to show the validity of using a coated-wall flow tube at ambient pressure and the data evaluation method based on the Monte Carlo model. Thus, previously published studies allow direct comparison and verification of our technique and the new modeling approach. Additionally, differences between previous studies call to further constrain the error limits of the parameters describing this interaction.

Relation between Adsorption Kinetics and Thermodynamics

In this section, we introduce the basic parameters describing adsorption to ice and their relation to thermodynamics, as we use them further in this work. They are consistent with our previous, more extensive description[48] and the literature cited therein. Assuming a simple Langmuir-type adsorption process, where the adsorbed species do not react on the surface and where diffusion into the bulk is negligible, the adsorption of a gas-phase molecule on the surface is described by the surface accommodation coefficient, S_0 (dimensionless quantity). S_0 is defined as the probability that an impinging molecule is not scattered from the surface on a time scale of picoseconds but loses its translational degree of freedom and kinetic energy. It has also been termed the sticking coefficient, trapping probability, or adsorption coefficient. Note that S_0 is not the mass accommodation coefficient, which has been used with different definitions in the literature. When applied to uptake into liquids, mass accommodation involves also solvation of the adsorbed molecule at a liquid surface.[54] Note that S_0 and the term mass accommodation coefficient have not been consistently used in previous studies about uptake processes on ice. S_0 allows the definition of an adsorption rate constant, k_a (in m s^{-1}), by the flux of molecules to the surface with the mean thermal velocity, $\tilde{\varpi}$ (m s^{-1}), as

$$k_a = \frac{S_0 \tilde{\varpi}}{4} \tag{1}$$

The adsorbed molecule can then thermally desorb back to the gas phase, for which the first-order rate constant, k_d (s^{-1}), in its most simple form can be given by the frequency with which the adsorbed molecules vibrate on the surface, τ_0 (s), the adsorption enthalpy, ΔH_{ads} (J mol^{-1}), the gas constant, R (J K^{-1} mol^{-1}), and the temperature, T (K)[55].

$$k_d = \frac{1}{\tilde{\tau}} \tag{2}$$

$$\tilde{\tau} = \tau_0 \, e^{-\Delta H_{ads}/RT} \tag{3}$$

When the concentration of surface-adsorbed molecules, $[X]_s$ (molecules per m^2), is in equilibrium with the gas-phase concentration in the immediate vicinity of the surface, $[X]_{gs}$ (molecules per m^3), the rate of adsorption can be equated to the rate of desorption, which leads to the well-known Langmuir equilibrium

$$k_a[X]_{gs}(1 - \theta_X) = k_d \theta_X [\text{sites}] \tag{4}$$

where [sites] denotes the maximum number of adsorption sites (per m^2) and θ_X is the fractional surface coverage, defined by $\theta_X = [X]_s/[\text{sites}]$. For a low coverage, i.e., if $1 - \theta_X \approx 1$, the gas−liquid partitioning is calculated from eq 4

$$\frac{\theta_X}{[X]_{gs}} = \frac{k_a}{k_d[\text{sites}]} \equiv K \tag{5}$$

This equation defines the Langmuir constant, K (m^3). For energetic calculations, the pressure $p_0 = 1$ atm is generally chosen as standard state for a molecule in the gas phase in atmospheric chemistry. An equivalent standard state can be derived for the adsorbate as suggested by Kemball and Rideal.[56] The principal idea behind this standard state is to fill an ideal gas with the molar volume $V = 2.24 \times 10^4$ cm^3 and with the

pressure $p_0 = 1$ atm into a thin layer of thickness $d_0 = 6$ Å, which represents the adsorbed state. In this layer, the gas covers the area $A = V/d_0 = 3.7 \times 10^{11}$ cm^2, corresponding to the surface concentration of $[X]_{s,0} = N_A/A$.

The pressure in this thin layer is $p_L = [X]_s A/VRT$. This pressure change leads to a change in the Gibbs free energy of the adsorbate, G_L, relative to the gas phase, G_g, given by $G_L = RT \ln(p_L/p_0)$. Adding the free energy for the adsorbate−surface interaction, ΔG^0_{ads}, to G_L, we obtain the free energy of the adsorbate, G_S. Using the equilibrium condition $G_s = G_g$ and converting the pressures to concentrations, we find

$$\frac{[X]_{gs}}{[X]_g}\frac{A}{V} = \exp\left(\frac{\Delta G^0_{ads}}{RT}\right) \equiv K_p^0 \quad (6)$$

and define the standard adsorption equilibrium constant K^0_p.

Equation 7 readily relates the adsorption enthalpy, ΔH_{ads} (J mol^{-1}), and standard entropy, ΔS^0_{ads} (J K^{-1} mol^{-1}), to K^0_p by using the thermodynamic relation $G = H - TS$.

$$-RT \ln K_p^0 = \Delta H_{ads} - T\Delta S^0_{ads} \quad (7)$$

Furthermore, comparison of eq 7 with the definition of the Langmuir constant K (eq 5) yields a relation between K and K^0_p

$$K = K_p^0 \frac{V}{A}\frac{1}{[\text{sites}]} \quad (8)$$

In conclusion, K and K^0_p describe the thermodynamics of the gas surface partitioning. It is noteworthy that the product of S_0 and τ_0 can be related to ΔS^0_{ads}. Combining eqs 1−3 and 5−9 and rearranging allows expressing the entropy change as function of the product of S_0 and τ_0.

$$\Delta S^0_{ads} = R \ln\left(\frac{S_0 \tilde{\omega} \tau_0 A}{4V}\right) \quad (9)$$

Hence, the partitioning and its temperature dependence of a species between the gas phase and a surface can be described by different sets of variables. One choice is using ΔH_{ads} and ΔS^0_{ads}; alternatively we can use the product of S_0 and τ_0 and the enthalpy, ΔH_{ads}.

Monte Carlo Simulation of Transport in Laminar Flow

In this section, we describe the basic concept of the Monte Carlo model to calculate the transport in the laminar flow of a cylindrical flow tube. We have developed a slight modification of a Monte Carlo model as originally suggested by Zvára.[43] The central idea of the Zvára model is to parametrize the microscopic processes of desorption from the surface and the random walk of an individual molecule through the gas phase to the next adsorption on the surface by a three-step process as follows (Figure 1). Desorption is followed by a random flight of one mean free path in length. Most desorbing molecules will hit the wall again after only a few collisions with gas-phase molecules. As the gas velocity of the laminar carrier gas flow close to the wall is vanishingly small and diffusion occurs in any direction, the molecule does not significantly change its position. It rather undergoes hopping in place in such repeated adsorption−desorption cycles. Only a small fraction of molecules will diffuse far enough into the laminar flow to be carried over a significant distance along the tube. Therefore, the macroscopic random walk of individual molecules consists of (i) the first encounter with the wall, (ii) the time of hopping in place, and (iii) long jumps until the next encounter with the wall, as shown in Figure 1.

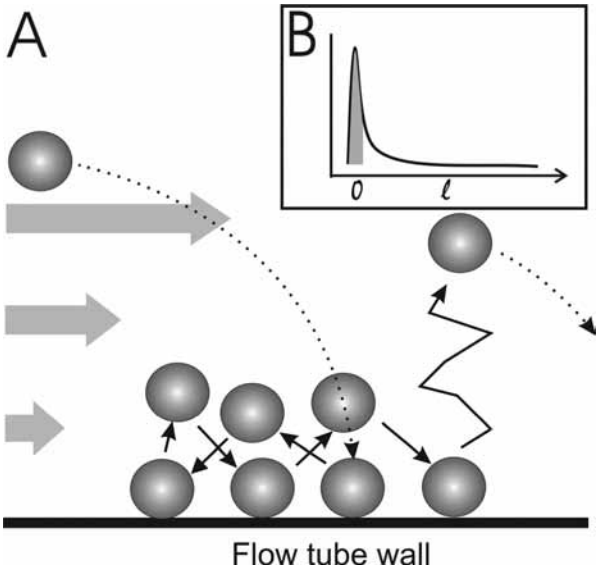

Figure 1. (A) Illustration of the transport process in the coated-wall flow tube. The first encounter with the wall is kinetically limited by diffusion across the laminar flow profile; once a molecule is within a mean free path distance from the wall, it undergoes repeated adsorption−desorption cycles without significant transport along the tube; only a few molecules can diffuse back into the flow tube, where the gas flows faster and the molecules make rare long jumps. (B) Probability density distributions for displacements (l) after desorption from the wall. In the present parametrization, the small displacements (marked in gray) are replaced by a random number of hops at the same position, while the remainder is approximated by a new distribution of long jumps after desorption from the wall. In the present parametrization, small displacements (marked in gray) are simulated by a random number of hops at the same position, while the tail in the probability distribution models the long jumps.

The first encounter of a gas-phase molecule with the wall is modeled using the first-order approximation of the known solution of the diffusion-controlled flux to the walls in a cylindrical laminar flow tube.[37] Equation 10 gives the first term of the exponential probability density function of the random distance (l in m) that the molecules are transported in the carrier gas stream before they encounter the wall for the first time. Here, $\tilde{\eta}_1$ (m) is the average distance (eq 11), where D (m^2 s^{-1}) is the diffusion coefficient and Q (m^3 s^{-1}) is the carrier gas volume flow rate. The invariable eigenvalue $\beta = 3.65$ and the preexponential coefficient $\alpha = 0.82$ are taken from of the first term of Gormley and Kennedy's continuum solution.[37]

$$\rho_1(l) = \frac{\alpha}{\tilde{\eta}_1} \exp^{-l/\tilde{\eta}_1} \quad (10)$$

$$\tilde{\eta}_1 = Q/\beta\pi D \quad (11)$$

At the average distance $\tilde{\eta}_1$, the molecule adsorbs for the first time at the wall and experiences a random number of adsorption−desorption cycles without being significantly transported by the carrier gas stream, which flows very slowly at the tube walls. The time that the molecule spends with this hopping is given by the product of the adsorption time per event ($\tilde{\tau}$ in s, eq 3), the mean number of successful adsorptions of an individual molecule per unit length segment of a cylindrical tube (ν in m^{-1}, eq 12), and the average length of the long jumps ($\tilde{\eta}$ in m, eq 14).[43] Equation 12 expresses ν by the surface accommodation coefficient, S_0, the radius of the flow tube, r,

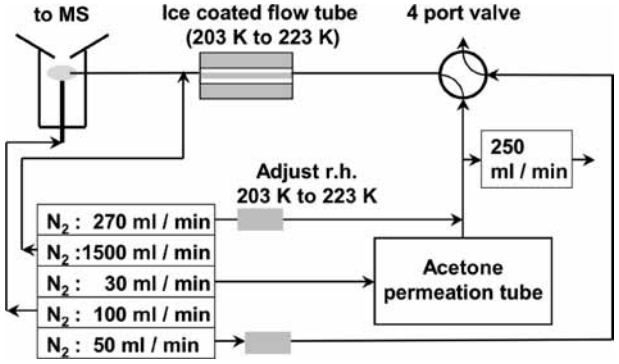

Figure 2. Experimental setup consisting of a coated-wall flow tube at atmospheric pressure, an acetone permeation source, and a mass spectrometer to monitor the acetone concentration with time. Note that the humidified carrier gas stream through the column was constant, whether acetone was turned on or off.

the volume flow rate, Q, the gas constant, R, the temperature, T, and the mass of a mole, M.

$$\nu = S_0(r/Q)\sqrt{(2\pi RT/M)} \tag{12}$$

Assuming a first-order desorption process, the time a molecule spends hopping in these repeated adsorption−desorption cycles is given by eq 13. Therein, $\tilde{\tau}$ and $\tilde{\eta}$ denote the average adsorption time and average jump length, respectively, and τ and η the individual adsorption times and jump lengths chosen randomly.

$$\rho_2(\nu\tau\eta) = \frac{1}{\nu\tilde{\tau}\tilde{\eta}} \exp^{-\nu\tau\eta/\nu\tilde{\tau}\tilde{\eta}} \tag{13}$$

Summarizing the many individual encounters with the wall in the probability density ρ_2 is the central idea of the model to enhance the calculation speed of the model. The average jump length along the flow tube of molecules that leave the layer close to the wall and diffuse into the laminar carrier gas flow ($\tilde{\eta}$ in m, eq 14) and the associated probability density function (eq 15) have been derived, based on the proposed probability distribution for displacements (Figure 1B) and on the exact solution of a chromatographic zone profile.[43] This profile takes into account axial diffusion and a nonuniform velocity profile in the flow tube.

$$\tilde{\eta} = \frac{\pi r^2 D}{Q} + \left(11 - 16\left[\frac{(\pi r^2/Q)}{(\pi r^2/Q) + \nu\tilde{\tau}}\right] + 6\left[\frac{(\pi r^2/Q)}{(\pi r^2/Q) + \nu\tilde{\tau}}\right]^2\right)\left(\frac{Q}{24\pi D}\right) \tag{14}$$

$$\rho_3(\eta) = \frac{1}{\tilde{\eta}} \exp^{-\eta/\tilde{\eta}} \tag{15}$$

Experimental Section

Flow Tube. The interaction of acetone with ice surfaces was investigated using a coated-wall flow tube at atmospheric pressure combined with an atmospheric pressure chemical ionization mass spectrometer (MS) described previously[24] (Figure 2).

The coated-wall flow tube consisted of a 72-cm-long, 0.6-cm-inner-diameter Pyrex tube inserted into a glass jacket kept at temperatures between 223 and 203 K. The pressure in the flow tube was kept at ambient pressure, typically 960 mbar. Under the experimental conditions reported here, no significant temperature gradient (<1 K) was detected along the column. The acetone trace gas was dosed to a bulk N_2 flow of which 50 mL/min were fed into the coated-wall flow tube to yield a concentration of 13 ppb acetone in the gas flow through the tube. The main gas flows were humidified to match the vapor pressure of ice at the temperature of the experiment to avoid net evaporation of or rimming on the ice surface. The ice surface was prepared by slowly freezing water at the inner surface of the Pyrex tube. For this, the Pyrex tube was cleaned with 5% aqueous HF solution, followed by thorough rinsing with Milli-Q water. Finally, the tube was wetted with Milli-Q water and quickly placed into a jacket at 258 K. The tube was rotated until a thin, hardly visible ice film froze within a few minutes.[26] The tube was than cooled to the desired temperature of 203, 208, 213, or 223 K. To ensure reproducibility, experiments were repeated 2, 1, 5, or 2 times at the different temperatures, respectively. A particular ice coating was used for a maximum of three measurements. The arrival of acetone after passage through the coated-wall flow tube is monitored by feeding the gas directly into the chemical ionization (CI) region of the mass spectrometer, where water cluster ions from a corona discharge act as CI reagents. The entire flow system up to the CI region in the MS was made of perfluoro-alkoxy copolymer (PFA Teflon) tubing so that faster response times could be achieved than in the study by Guimbaud et al.[24] The mass spectrometer monitored the acetone-proton cluster $H^+(CH_3COCH_3)$ with m/z = 59 and water-proton cluster $H^+(H_2O)_3$ with m/z = 55. Monitoring these two major proton clusters rather than the complete cluster spectrum as in the study by Guimbaud et al.[24] resulted in an improved overall signal-to-noise ratio. The ratio of the $H^+(CH_3COCH_3)$ and $H^+(H_2O)_3$ signals was confirmed to be proportional to the acetone concentration.

Monte Carlo Simulation. The simulations were run in Maple version 9.0 and took approximately 10 min each for 1000 and 3 h for 10 000 molecules on a Macintosh G4 550 and yielded a concentration profile with time under the given experimental conditions. In a single run, the time that each molecule needs to pass the coated-wall flow tube (retention time) was determined by repeating the basic steps of the random walk described above (hopping at one position, long jumps) until the molecule reached the end of the tube. The resulting distribution of retention times was then converted into a histogram, representing the experimentally derived uptake traces. For this, the time the molecule spends hopping at one position and the length of the long jumps were chosen randomly from the corresponding probability density functions ρ_2 and ρ_3 (eqs 13 and 15), respectively. The length of the jump to reach the wall for the first time behind the entrance of the tube was chosen randomly from the distribution provided in eq 10. The room-temperature value of the diffusion coefficient of acetone in N_2 (0.11 cm^2 s^{-1}) was taken from Andrussov.[57] The exponent of the temperature dependence was set to 1.75 (Results and Discussion). The times needed to travel the lengths of the jumps were calculated based on the average flow velocity. To derive ΔH_{ads}, simulations were repeated with varying ΔH_{ads} for a specific choice of ΔS_{ads} (Results and Discussion) while the other input parameters were fixed to meet the experimental conditions, until the gained histogram fit the experimental uptake curve.

To test the performance of the Monte Carlo simulation, a modified simulation code was used in which all parameters controlling transport and diffusion in laminar flow were as in the original code but which contained an irreversible adsorption step, in which the residence time in the adsorbed state was set to infinity. In this case, each successful collision with the surface (i.e., with a certain probability S_0) led to the loss of the molecule

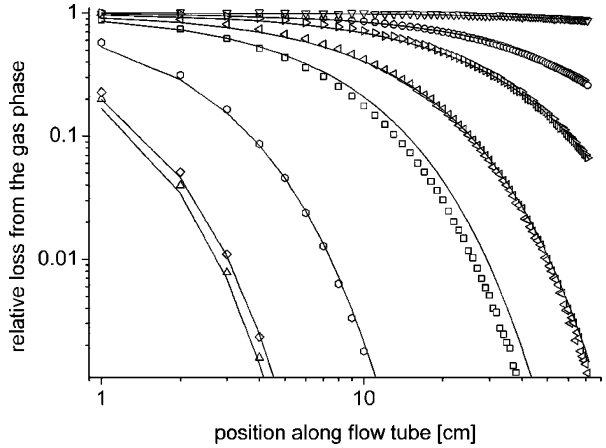

Figure 3. Performance test of the Monte Carlo simulation used in this study. The loss of a species from the gas phase along the flow tube at atmospheric pressure assuming an irreversible loss at the wall. Comparison of the Monte Carlo model (symbols) and CKD solution (lines, see text) for different surface accommodation coefficients, S_0.

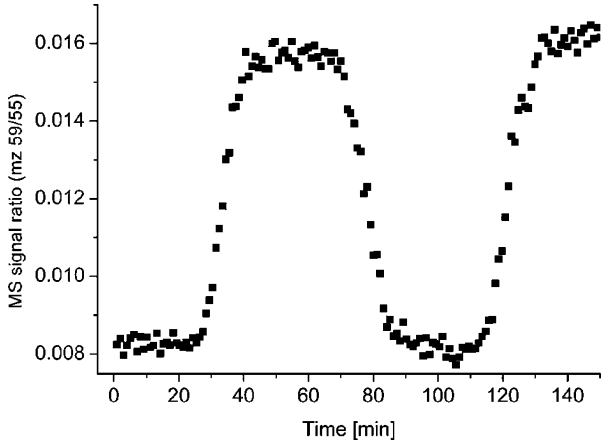

Figure 4. Measured mass spectrometer signals of acetone concentration at the outlet of the ice-coated-wall flow tube as a function of time at 213 K. The acetone was switched on at time 0, switched off at 60 min, and switched on again at about 90 min.

from the gas phase, and the position where this occurred was recorded for each molecule. We believe that this provides a good test of the simulation features in the regime of combined diffusion and first-order loss to the tube wall. For this case, also analytical solutions of the diffusion equation for a laminar cylindrical flow tube including a first-order loss process at the surface are available in the literature. We compared our results with the solution derived by Cooney, Kim, and Davis[44] (further referred to as CKD solution). The CKD solution has originally been used for a similar purpose by Murphy and Fahey,[58] and for this study, we have used an implementation described in our recent flow-tube study.[59] It describes the loss of gas-phase molecules to the walls of a cylindrical laminar flow tube as a function of the surface accommodation coefficient, S_0, at the wall.

Results and Discussion

Figure 3 shows the results of the performance test of the Monte Carlo simulation, for a range of uptake coefficients, which were simulated by variation of the surface accommodation coefficient S_0 and by assuming a very low desorption rate to mimic irreversible uptake. The solid lines were obtained using the CKD solution. The comparison was made at room temperature to avoid any discrepancy in handling temperature-dependent quantities. The Monte Carlo and the analytical solutions agree remarkably well in view of the simple way the Monte Carlo simulation parametrizes the combined transport and diffusion along the tube. The chromatographic zone profile used to derive eq 14 also takes into account axial diffusion. On the basis of this comparison, we are very confident that individual trajectories for the case of reversible adsorption (where successful adsorptions are followed by desorption and further hops and jumps) are very well-represented in the model, especially in the range that is affected by both adsorption kinetics and diffusion.

Figure 4 shows a breakthrough curve of acetone on ice at a temperature of 213 K. Initially, a steady flow of carrier gas is passed through the flow tube, which gives rise to stable MS signals of $H^+(H_2O)_3$ clusters at $m/z = 55$ (not shown). At time $t = 0$, the acetone was turned on and started to interact with the ice surface. Until approximately 40 min when the gas-phase concentration at the tube's exit reached a stable value, this interaction led to a net accumulation of acetone on the surface to establish equilibrium. When the acetone in the carrier gas is turned off, the decay of the signal can be observed until the acetone is completely removed from the surface. Within the experimental error, the integrated areas above and under the adsorption and desorption profiles, respectively, are identical, implying that the uptake of acetone on the ice is fully reversible within the time scale and precision of this experiment. The symmetry of both profiles is also an indication that diffusion of acetone into the ice does not occur within the time scale and sensitivity of the experiment, which is in agreement with the previous studies on this system as cited above. Therefore, the profiles describe the uptake of acetone to ice until the rate of adsorption and desorption match at equilibrium and no net uptake is observed.

Figure 5 shows experimental and simulated profiles at different temperatures. For plots A and C, those two experimental traces were selected that exhibited the lowest and highest retention times from all experiments available at that temperature, respectively. Note that the length of the ice film was equal in all experiments. This should indicate the variability observed among different ice films compared to the difference between experiment and simulation or compared to the effect of changes in the driving variables on the simulation outcome. The freedom in choosing the fundamental parameters was first constrained by taking the experimentally observed standard adsorption entropy of -101 J mol^{-1} K^{-1} [31] to fix the product of S_0 and τ_0 to 4.3×10^{-15} s, according to eq 9. ΔS^0_{ads} has been retrieved from a temperature series of packed bed experiments as reported previously.[31] Then, the profiles were adjusted to the experimental data by varying ΔH_{ads}. The profiles with values for ΔH_{ads} of -46.48 and -46.91 kJ mol^{-1} at 203 K are shown in Figure 5A (solid lines), -45.99 kJ mol^{-1} at 208 K (Figure 5B), -46.11 and -46.66 kJ mol^{-1} at 213 K (Figure 5C), and -46.66 kJ mol^{-1} at 223 K (Figure 5D). Typical characteristics of trajectories in the simulations were as follows (for 208 K). The number of collisions along the tube was 2.4×10^4 cm^{-1}; the average length of long jumps was 0.6 cm; the average number of hops at one position was about 122; the average residence time (with respect to a single desorption event) was, for example, 0.18 s at 208 K assuming ΔH_{ads} of -46 J mol^{-1} and τ_0 of 5×10^{-13} (see below). Apart from the surface residence time, $\tilde{\tau}$ (cf. eq 3), these quantities are only weakly temperature-dependent. The temperature-dependent position of the signal rise is mainly driven by the surface residence time.

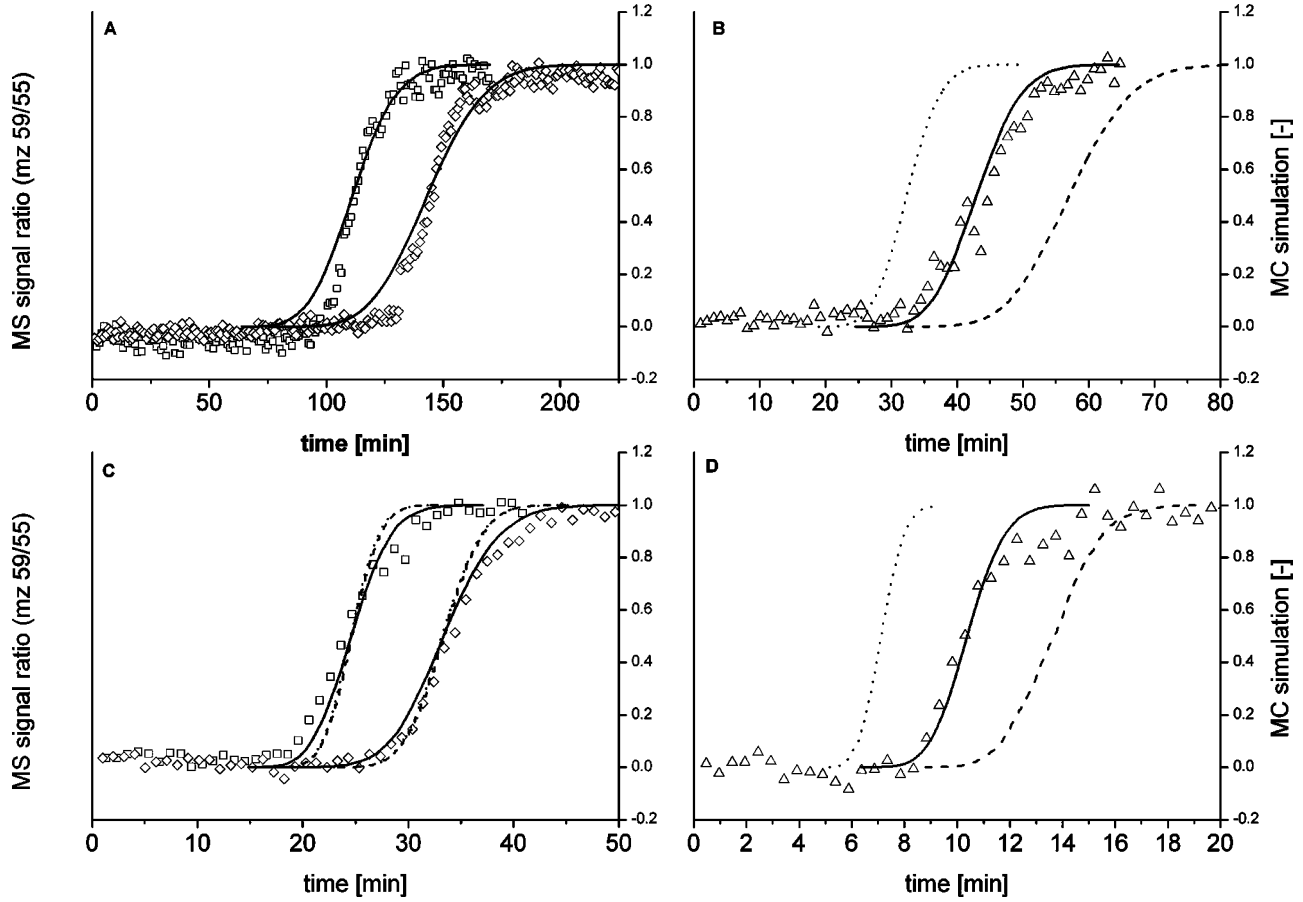

Figure 5. Breakthrough curves of acetone as measured with the mass spectrometer at different temperatures (squares). Note the changing *x*-axis scale in part A at 203 K, B at 208 K, C at 213 K, and D at 223 K. At 213 and 203 K, several experiments were conducted, and the two extreme profile curves are plotted to determine the influence of experimental scatter on the adsorption enthalpy. The simulations that best fitted the experiments are also plotted (black lines). The influence of the adsorption enthalpy is illustrated in part B, where a simulated profile with change in the adsorption enthalpy of -0.5 kJ mol^{-1} (dotted line) and $+0.5$ kJ mol^{-1} (dashed line) are shown. In part C, the dotted and dashed lines result from simulations where the probability density functions of η and of $\nu\tau\eta$ were varied. See text for details.

As evident from Figure 5 (solid lines), the simulations could easily be adjusted to the experimental data by using ΔH_{ads} as the only free variable (keeping S_0 and τ_0 fixed and using 101 J mol^{-1} K^{-1} for the entropy). In general, the rising signal profiles are well-reproduced, and also the temperature-dependent position is well-simulated with consistent ΔH_{ads} values. This indicates that, analogous to the conclusions drawn from other experimental methods applied to the acetone−ice interaction, the adsorption and desorption processes are reasonably well-parametrized within the framework used here. It further suggests an adsorption mechanism controlled by hydrogen bonds of uniform strength and indicates that the assumptions of Langmuir-type adsorption and laminar flow correctly describe the processes in the flow tube. Yet, Figure 5 also indicates that at lower temperatures the shape of the experimental curve was slightly steeper than the simulated one and vice versa for the higher temperatures. In the following, we will first discuss the parameters that influence simultaneously the shape and position of the simulated curve. Second, we discuss some parameters that might explain the slight derivation between the experimental and simulated curve shapes.

The key variables that determine the shape and position of the simulated profiles are (1) the variable $\tilde{\eta}$ and the product of $\nu\tilde{\tau}\tilde{\eta}$ or equivalently ΔG^0_{ads} and (2) the accepted probability density function of η and $\nu\tau\eta$. In this work, ΔG^0_{ads} has been expressed in terms of the dependent variables ΔH_{ads} and ΔS^0_{ads}. Figures 5A−C illustrate that a small change in ΔH_{ads} at constant ΔS^0_{ads} simultaneously leads to a significant change in the profile's position and to a small change in the slope, resulting in a very small scatter of ΔH_{ads} driven by the variance in the experimental profiles. The dashed lines in Figure 5B indicate the simulation results when ΔH_{ads} of -46 kJ mol^{-1} was set higher or lower by 500 J mol^{-1}. Therefore, the overall error in determining ΔH_{ads} from adjusting the simulation to the experimental data is mainly driven by variations from experiment to experiment shown in Figures 5A and 5C rather than by degrees of freedom in adjusting the individual simulation. In a similar way, to determine the influence of ΔS^0_{ads}, the simulations shown in Figure 5D were rerun with values of ΔS^0_{ads} changed by about 3 J K^{-1} mol^{-1} up and down from 101 J K^{-1} mol^{-1} (corresponding to $S_0 \times \tau_0 = 6 \times 10^{-15}$ s and 3×10^{-15} s, respectively), while keeping ΔH_{ads} constant. When these simulations with changed ΔS^0_{ads} were readjusted to the experimental data by changing ΔH_{ads}, the shape of this simulation did not differ significantly from the original one (solid line) as expected based on the relation $\Delta G^0_{ads} = \Delta H_{ads} - T\Delta S^0_{ads}$. Therefore, the error in the ΔH_{ads} values is strongly linked to the error of the entropy value (or to that of S_0 and τ_0). The experimental error associated with ΔS^0_{ads} for acetone on ice is 16 J mol^{-1} K^{-1},[31] which then results in a variation of ± 3 kJ mol^{-1} in ΔH_{ads}.

It is interesting to note that, while the model reproduces the profiles well, there is a small systematic deviation between model and experiment. At lower temperatures, the experimental slopes are steeper than the model, while this is the other way

around at higher temperatures. When considering how to improve the simulation's outcome regarding the slope of the curve at different temperatures, the first parameter that comes to one's mind is the temperature dependence of the diffusion coefficient. After all, the choice of the temperature dependence of the diffusion coefficient used in this work was somewhat arbitrary. However, when the exponent therein rather drastically changed between 1.5 and 2.0, the maximum acceptable range,[58] no change in the shape and no relevant change in the position of the profiles were obtained (simulations not shown). The only way to get steeper profiles as observed at 203 K was by artificially narrowing the probability density functions of η and $\nu\tau\eta$. The two dashed lines in Figure 5C were obtained by replacing one of the two probability distributions by the average values $\tilde{\eta}$ and$\nu\tilde{\tau}\tilde{\eta}$, respectively, and keeping all other parameters constant. This drastic narrowing did not change the position of the turnover point of the simulated profiles but shows that the width of the distributions has quite a significant effect on the kinetics of a profile. The width of the distributions is either related to the transport processes in the gas phase (in the case of η) or to the adsorption and desorption process (in the case of τ). A narrower distribution of the jump lengths could indicate a distortion of the laminar flow profile toward plug flow, eventually induced by small scale eddies near the wall due to a not perfectly smooth ice surface. However, we do not believe that the conditions for laminar flow do change significantly as a function of temperature. Also, any other systematic errors in describing the transport in the gas phase, such as the interplay of the laminar flow profile and the gas-phase diffusion should not depend on temperature. Thus, the observed temperature-dependent deviation between experiment and model is most probably due to the ice−acetone interaction. For example, the nature of adsorption processes critically depends on the available number of hydrogen bonds, which has been shown to change with temperature at temperatures as low as 200 K,[60] using surface-sensitive nonlinear optics techniques. This would then lead to a temperature dependence of τ_0 in our simple model behind eqs 2 and 3 and subsequently affect the distribution of the τ values. Furthermore, a small deviation from the first-order desorption behavior could also have an impact on the width of this distribution. Also, the adsorption−desorption process may occur at adsorption sites that differ in the adsorption strength. The high water mobility on the ice surface ensures that the uniformity of adsorption sites is satisfied at high temperatures. This is one of the critical assumptions in the Langmuir model. Yet, as the temperature gets lower, the ice surface becomes more rigid,[25,61−63] and this assumption might be less well-obeyed. Thus, one might speculate that the temperature-dependent deviation between the simulation outcome and the experimental results could be related to the temperature-dependent changes of the ice surface structure.

The parametrization of the Monte Carlo simulations depends only on the product of τ_0 and S_0, which is also linked to the value of the entropy change (eq 9), and there is no indication from the experiments showing an independent response of the breakthrough to either of τ_0 or S_0. According to the simplified picture of transport in the flow tube, which formed the basis of our simulations, this constraint is also given by the fact that both the time a molecule spends hopping as well as the mean jump length are dependent on the product of τ_0 and S_0. This seems then to be an inherent feature of all laminar flow-tube techniques where the forward velocity close to the wall is small and the number of collisions is very large, making it virtually impossible to independently determine τ_0 and S_0.

ΔS^0_{ads} was taken here from an independent study but could in principle also be estimated from simultaneously simulating the breakthrough curves at different temperatures. In any case, if τ_0 and ΔS^0_{ads} are known, then S_0 can be estimated from eq 9. Taking the experimentally determined value of $\Delta S^0_{ads} = -101 \pm 16$ J K^{-1} mol^{-1} and an estimated range of $\tau_0 = 1 \times 10^{-12}$ to 1×10^{-13} s,[25,62,63] a range for S_0 from 0.004 to 0.043 can be suggested. This is to our knowledge the first estimate of S_0 for acetone on ice. It is important to point out that this range of S_0 is just a rough estimate, as there has been some discussion on the validity to describe the preexponential factor in eq 3 by a arbitrarily chosen phonon frequency.[64] Note that the Monte Carlo simulation presented here is free of this assumption about τ_0.

When the data presented here are reanalyzed using a van't Hoff plot of the standard equilibrium constant (i.e., $\ln(K^0_p)$) versus $1/T$ as described in our previous work,[31] i.e., by application of eq 16, an adsorption enthalpy is obtained from the slope of a regression line. This analysis of the data set with this independent method that is frequently used in packed bed experiments serves to identify the influence that gas-phase diffusion has on the experimental result. Note that the Monte Carlo model parametrized gas-phase diffusion, while eq 16 analysis neglects it. At low coverage, K^0_p can also be deduced from the retention time (t_r) according to eq 16 where t_m is the carrier gas holdup time, t_r^{sys} is the retention time of acetone in the flow system before and after the column, a/υ is the surface area to volume ratio in the column, and V/A is the standard volume and surface area.

$$K_p^0 = \frac{(t_r - t_r^{sys}) - t_m}{t_m} \frac{\upsilon A}{aV} \tag{16}$$

This analysis, for which t_m was set to 97 s and t_r^{sys} to 5 s, yields ΔH_{ads} of -52 kJ mol^{-1}. While this analysis can only serve as rough estimate due to the limited number of measurements at different temperatures and consequently low quality of the regression line, the reasonable agreement of both results might imply that diffusion in the gas phase plays only a minor role in the retention of acetone in the coated-wall flow tube at atmospheric pressure. This conclusion also holds for $\Delta S^0_{ads,}$ for which a value of -87 J K^{-1} mol^{-1} is obtained from the intercept of the linear regression and which is in fair agreement to our previous result of -101 ± 16 J K^{-1} mol^{-1}. Recent work by Behr et al., however, gives $\Delta S^0_{ads} = -51 \pm 12$ J K^{-1} mol^{-1} for the adsorption of acetone on ice.[65] In this latter study, the ice was generated by depositing water molecules from the gas phase; thus the deviating results might in part be due to different uncertainties in the determination of the surface area of the ice used in both experiments.

Apart from serving as a test of this type of flow tube analysis at atmospheric pressure, this study also provides another ΔH_{ads} value of acetone on ice of -46 ± 3 kJ mol^{-1}, which is in reasonable agreement with all other studies of this interaction reported so far at temperatures typical for the upper troposphere and at low surface coverage (θ): Dominé and Rey-Hanot,[53] -55 ± 7 kJ mol^{-1} (0.03% $< \theta <$ 7%; 193 K $< T <$ 213 K); Bartels-Rausch et al.,[31] -52 ± 2 kJ mol^{-1} (0.1% $< \theta <$ 6%; 193 K $< T <$ 223 K); Winkler et al.,[29] -46 ± 7 kJ mol^{-1} (0.003% $< \theta <$ 4%; 198 K $< T <$ 218 K); Peybernès,[30] -49 ± 7 kJ mol^{-1} (0.2% $< \theta <$ 100%; 193 K $< T <$ 223 K). It is worth noting that the studies by Dominé and Rey-Hanot, Peybernès, Winkler, and this work were conducted with ice samples prepared following exactly the same protocol, and thus differences in

the ice surface structure should be negligible. Consequently, the span of experimentally derived ΔH_{ads} from -46 to -55 kJ mol^{-1} might not be attributed to a deviating number of surface defects or similar surface structure features. Following the result of our previous study, acetone adsorption on aged or annealed ice or snow samples does not significantly respond to ice freezing protocol or temperature history.[31] It is also interesting to note that the coated-wall flow-tube experiments by Winkler, Peybernès, and this work with a very similar geometric setup yield a closer agreement of the resulting ΔH_{ads} compared to the results of a chromatographic method used by Bartels-Rausch and of a adsorption isotherm method described by Dominé. This might hint to yet undefined systematic experimental errors in each setup causing the span of reported ΔH_{ads} values. Even though no indication of varying ΔH_{ads} with surface coverage is evident from the compilation presented above, varying surface coverage might at least partially contribute to each method's systematic error. Indication for this conclusion came from Winkler et al., who suggest a trend of lower values of ΔH_{ads} at higher coverage even below a surface coverage of 0.07% based on analysis of a restricted data set and by referring to molecular dynamics and ab initio calculations.[51,52] The surface coverage of acetone in our experiments can be estimated from the times taken from Figure 5 at which the net adsorption to the surface was complete and a concentration of 13 ppb acetone in the carrier gas: 0.5% at 223 K, 1.2% at 213 K, 1.8% at 208 K, and 5.2% at 203 K. For this analysis, we make the assumptions that the ice films are neither rough nor porous, that the geometric inner surface area of the tube is identical to the ice surface probed by the acetone molecules, and that the maximum surface coverage of acetone on ice is 2.7×10^{14} molecules per cm^2 as determined by Winkler et al.[29] The surface coverage and temperature were not varied independently as the influence of surface coverage on the partitioning of acetone was beyond the scope of this work. In future experiments, it might be interesting to monitor the partitioning of acetone on ice with decreasing surface coverage at a fixed temperature to further address this topic.

Conclusion

An atmospheric pressure variant of the coated-wall flow-tube technique was presented and applied to investigate the reversible adsorption of acetone on ice. The main feature of this method is to simulate experimental breakthrough curves by a Monte Carlo method, which uses a simplified model of transport in laminar flow. Under conditions of simple first-order wall loss, the simulation agrees very well with an analytical solution of the diffusion equation. For the case of reversible adsorption, the simulations allow the retrieval of an adsorption enthalpy of -46 ± 3 kJ mol^{-1} for acetone on ice, which is in good agreement with other static and flow tube methods. While the overall performance of the simulation to reproduce experimental breakthrough curves was very good, the temperature dependence of the curve's slope did match less perfect. We argued that this is neither due to the physical parametrization of partitioning nor to the simulation variables. We argued that the small temperature-dependent deviation from the simulated profiles indicates changes in the adsorption properties with changing temperature. This also demonstrates that the profiles very sensitively respond to such changes. The study also shows that as soon as uptake traces measured in laminar flow tubes are significantly affected by the adsorption equilibrium (due to a large enough number of wall collisions), microkinetic param eters, such as the surface accommodation coefficient or the surface residence time, cannot be independently determined.

The Monte Carlo model is very simple to use and efficient with respect to CPU-time usage compared to other numeric continuum methods. It also does not depend on a rather arbitrary choice of the preexponential factor describing the desorption kinetics, as frequently done in similar studies. We have argued that these parameters can rather be derived from ΔS^0_{ads} that has been determined in independent experiments. It can be easily extended to include further processes on the surface or in the gas phase.

Acknowledgment. This work was part of a project by the European Commission (CUT-ICE: EVK2-CT1999-00005) and was funded by the Swiss Federal Office for Education and Science (99.00491-2). We thank M. Birrer for his excellent technical support of this work and for help in construction of the mass spectrometer.

References and Notes

(1) Couch, T. L.; Sumner, A. L.; Dassau, T. M.; Shepson, P. B.; Honrath, R. E. *Geophys. Res. Lett.* **2000**, *27*, 2241.
(2) Dubowski, Y.; Colussi, A. J.; Boxe, C.; Hoffmann, M. R. *J. Phys. Chem. A* **2002**, *106*, 6967.
(3) Solomon, S. *Nature* **1990**, *347*, 347.
(4) Jaeglé, L.; Jacob, D. J.; Brune, W. H.; Wennberg, P. O. *Atmos. Environ.* **2001**, *35*, 469.
(5) Wolff, E. W.; Bales, R. C. *Chemical Exchange between the Atmosphere and Polar Snow*; Springer: Berlin, Heidelberg, 1996; Vol. I43.
(6) Dominé, F.; Shepson, P. B. *Science* **2002**, *297*, 1506.
(7) Bottenheim, J. W.; Fuentes, J. D.; Tarasick, D. W.; Anlauf, K. G. *Atmos. Environ.* **2002**, *36*, 2535.
(8) Lindberg, S. E.; Brooks, S.; Lin, C. J.; Scott, K. J.; Landis, M. S.; Stevens, R. K.; Goodsite, M.; Richter, A. *Environ. Sci. Technol.* **2002**, *36*, 1245.
(9) Houdier, S.; Perrier, S.; Dominé, F.; Cabanes, A.; Legagneux, L.; Grannas, A. M.; Guimbaud, C.; Shepson, P. B.; Boudries, H.; Bottenheim, J. W. *Atmos. Environ.* **2002**, *36*, 2609.
(10) Guimbaud, C.; Grannas, A. M.; Shepson, P. B.; Fuentes, J. D.; Boudries, H.; Bottenheim, J. W.; Domine, F.; Houdier, S.; Perrier, S.; Biesenthal, T. B.; Splawn, B. G. *Atmos. Environ.* **2002**, *36*, 2743.
(11) Boudries, H.; Bottenheim, J. W.; Guimbaud, C.; Grannas, A. M.; Shepson, P. B.; Houdier, S.; Perrier, S.; Dominé, F. *Atmos. Environ.* **2002**, *36*, 2573.
(12) Grannas, A. M.; Shepson, P. B.; Guimbaud, C.; Sumner, A. L.; Albert, M.; Simpson, W.; Dominé, F.; Boudries, H.; Bottenheim, J.; Beine, H. J.; Honrath, R.; Zhou, X. L. *Atmos. Environ.* **2002**, *36*, 2733.
(13) Quinlan, M. A.; Reihs, C. M.; Golden, D. M.; Tolbert, M. A. *J. Phys. Chem.* **1990**, *94*, 3255.
(14) Golden, D. M.; Spokes, G. N.; Benson, S. W. *Angew. Chem., Int. Ed. Engl.* **1973**, *12*, 534.
(15) Caloz, F.; Fenter, F. F.; Tabor, K. D.; Rossi, M. J. *Rev. Sci. Instrum.* **1997**, *68*, 3172.
(16) Koch, T. G.; Fenter, F. F.; Rossi, M. J. *Chem. Phys. Lett.* **1997**, *275*, 253.
(17) Hanson, D. R.; Ravishankara, A. R. *J. Geophys. Res.* **1991**, *96*, 17307.
(18) Abbatt, J. P. D.; Beyer, K. D.; Fucaloro, A. F.; McMahon, J. R.; Wooldridge, P. J.; Zhang, R.; Molina, M. J. *J. Geophys. Res., Atmos.* **1992**, *97*, 15819.
(19) Lamb, D.; Clapsaddle, C. *Geophys. Res. Lett.* **1989**, *16*, 1173.
(20) Sommerfeld, R. A.; Conklin, M. H.; Laird, S. K., *J. Colloid Interface Sci.* **1992**, *149*, 569.
(21) Conklin, M. H.; Sommerfeld, R. A.; Laird, S. K.; Villinski, J. E. *Atmos. Environ., Part A* **1993**, *27*, 159.
(22) Goss, K. U. *Environ. Sci. Technol.* **1993**, *27*, 2826.
(23) Langenberg, S.; Schurath, U. *Geophys. Res. Lett.* **1999**, *26*, 1695.
(24) Guimbaud, C.; Bartels-Rausch, T.; Ammann, M. *Int. J. Mass Spectrom.* **2003**, *226*, 279.
(25) Bartels-Rausch, T.; Eichler, B.; Zimmermann, P.; Gäggeler, H. W.; Ammann, M. *Atmos. Chem. Phys.* **2002**, *2*, 235.
(26) Hynes, R. G. F.; Miguel A.; Cox, R. A. *J. Geophys. Res.* **2002**, *107*, 18.
(27) Huff, A. K.; Abbatt, J. P. D. *J. Phys. Chem. A* **2002**, *106*, 5279.
(28) Sokolov, O.; Abbatt, J. P. D. *J. Phys. Chem. A* **2002**, *106*, 775.
(29) Winkler, A. K.; Holmes, N. S.; Crowley, J. N. *Phys. Chem. Chem. Phys.* **2002**, *4*, 5270.
(30) Peybernès, N.; Marchand, C.; Le Calvé, S.; Mirabel, P. *Phys. Chem. Chem. Phys.* **2004**, *6*, 1277.

(31) Bartels-Rausch, T.; Guimbaud, C.; Gäggeler, H. W.; Ammann, M. *Geophys. Res. Lett.* **2004**, *31*, L16110.
(32) Conklin, M. H.; Sigg, A.; Neftel, A.; Bales, R. C. *J. Geophys. Res., Atmos.* **1993**, *98*, 18367.
(33) Huthwelker, T.; Lamb, D.; Baker, M.; Swanson, B.; Peter, T. *J. Colloid Interface Sci.* **2001**, *238*, 147.
(34) Abbatt, J. P. D. *Chem. Rev.* **2003**, *103*, 4783.
(35) Eichler, B.; Gäggeler, H. W.; Gäggeler-Koch, H. *Radiochim. Acta* **1979**, *26*, 193.
(36) Gäggeler, H.; Eichler, B.; Greulich, N.; Trautmann, N.; Herrmann, G. *Radiochim. Acta* **1986**, *40*, 137.
(37) Gormley, P. G.; Kennedy, M. *Proc. R. Ir. Acad.* **1949**, 163.
(38) Taylor, G. *Proc. R. Soc. London, Ser. A* **1953**, *219*, 186.
(39) Taylor, G. *Proc. R. Soc. London, Ser. A* **1954**, *223*, 446.
(40) Aris, R. *Proc. R. Soc. London, Ser. A* **1956**, *235*, 67.
(41) Walker, R. E. *Phys. Fluids* **1961**, *4*, 1211.
(42) Brown, R. L. *J. Res. Natl. Inst. Stand. Technol.* **1978**, *83*, 8.
(43) Zvára, I. *Radiochim. Acta* **1985**, *38*, 95.
(44) Cooney, D. O.; Kim, S. S.; Davis, E. J. *Chem. Eng. Sci.* **1974**, *29*, 1731.
(45) Msibi, I. M.; Shi, J. P.; Harrison, R. M. *J. Atmos. Chem.* **1993**, *17*, 339.
(46) Poirier, R. V.; Carr, R. W. *J. Phys. Chem.* **1971**, *75*, 1593.
(47) Ogren, P. J. *J. Phys. Chem.* **1975**, *79*, 1749.
(48) Ammann, M.; Pöschl, U.; Rudich, Y. *Phys. Chem. Chem. Phys.* **2003**, *5*, 351.
(49) Behr, P.; Terziyski, A.; Zellner, R. *Z. Phys. Chem.* **2004**, *218*, 1307.
(50) Fenter, F. F.; Caloz, F.; Rossi, M. J. *Rev. Sci. Instum.* **1997**, *68*, 3180.
(51) Picaud, S.; Hoang, P. N. M. *J. Chem. Phys.* **2000**, *112*, 9898.
(52) Marinelli, F.; Allouche, A. *Chem. Phys.* **2001**, *272*, 137.
(53) Dominé, F.; Rey-Hanot, L. *Geophys. Res. Lett.* **2002**, 29.
(54) Jayne, J. T.; Duan, S. X.; Davidovits, P.; Worsnop, D. R.; Zahniser, M. S.; Kolb, C. E. *J. Phys. Chem.* **1991**, *95*, 6329.
(55) Frenkel, J. *Z. Phys.* **1924**, *26*, 117.
(56) Kemball, C.; Rideal, E. K. *Proc. R. Soc. London, Ser. A* **1946**, *187*, 53.
(57) Andrussov, L. Diffusion. In *Landolt-Börnstein Data for Physics, Chemistry, Astronomy, Geology, and Technology*, 6th ed.; Springer: Berlin, 1969; Vol. II/5a, p 513.
(58) Murphy, D. M.; Fahey, D. W. *Anal. Chem.* **1987**, *59*, 2753.
(59) Gutzwiller, L.; George, C.; Rössler, E.; Ammann, M. *J. Phys. Chem. A* **2002**, *106*, 12045.
(60) Wei, X.; Miranda, P. B.; Shen, Y. R. *Phys. Rev. B* **2002**, *66*, 085401.
(61) Girardet, C.; Toubin, C. *Surf. Sci. Rep.* **2001**, *281*, 1.
(62) Eichler, B.; Zimmermann, H. P.; Gäggeler, H. W. *J. Phys. Chem. A* **2000**, *104*, 3126.
(63) Schaff, J. E.; Roberts, J. T. *J. Phys. Chem.* **1996**, *100*, 14151.
(64) L'vov, B. V. *Spectrochim. Acta, Part B* **1997**, *52*, 1.
(65) Behr, P.; Scharfenort, U.; Terziyski, A.; Zellner, R. *Pollutants and Environment*; **2005**, in press.